

A Rigorous Phase Noise Analysis of Tuned Ring Oscillators

Harish Krishnaswamy and Hossein Hashemi

Electrical Engineering - Electrophysics

University of Southern California,

Los Angeles, CA-90089, Email: hkrishna@usc.edu, hossein@usc.edu

Abstract—Tuned ring oscillators have found numerous applications due to their ability to generate multiple phases at high frequencies of operation while maintaining high signal purity. However, a comprehensive phase noise theory that explains the phase noise performance of tuned rings as a function of design parameters such as the number of elements and inter element phase shift is lacking. This paper rigorously builds such a theory and demonstrates that the phase noise improves by a factor of $10\log_{10}N$ as the number of elements (N) is increased. Further, the phase noise deteriorates (by a factor of $40\log_{10}\cos\Delta\phi$ at least) when the inter element phase shift $\Delta\phi$ is increased. In the context of multiple phase generation, under a fixed current budget, we demonstrate that it is beneficial to use a larger ring sizes. Extensive GHz-range simulations as well as measurements of prototype oscillators validate these claims.

Index Terms—Oscillators, phase noise, phase shifters.

I. INTRODUCTION

The multiple-phase generation capability of tuned ring oscillators has led to their application in the fields of wireless phased arrays [1], clock and data recovery [2] and quadrature LO generation for sideband rejection [3]. The tuned nature of the element loads improves the oscillator quality factor and enables higher frequencies of operation when compared to a ring oscillator with resistive loads [2].

While the phase noise of ring oscillators with resistive loads has been studied [4], a complete theory that details the dependence of the phase noise of tuned rings on design parameters such as the bias current, number of elements and inter element phase shift is missing. Such dependencies are critical to system trade-offs in the aforementioned applications that employ tuned ring oscillators. This paper develops such a theory. Section II presents a general model for tuned rings and a steady state analysis. Section III contains an extensive phase noise analysis based on a popular phase noise formulation [6]. Section IV presents extensive simulations and measurement results to validate the claims and Section V concludes the paper.

II. STEADY STATE ANALYSIS

Fig. 1(a) depicts the block diagram of a differential tuned ring oscillator. Each element of the ring consists of a nonlinear transconductance cell driving a parallel- RLC resonant load. An nMOS differential pair represents a possible implementation of the transconductance. The phase boundary condition depends on the manner in which the ring is closed. For example, the ring may be closed with a direct or inverted connection of the lines, resulting in phase boundary conditions of 0° and 180° respectively.

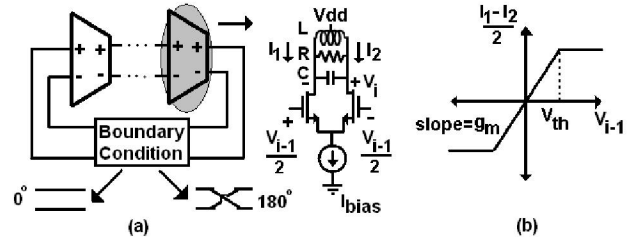


Fig. 1. (a) Differential tuned ring oscillator, with a possible MOSFET implementation (b) Piecewise linear model for the nonlinearity of the differential pair.

To obtain the steady state solution of the oscillator, the nonlinearity of the transconductance must be modelled. Fig. 1(b) shows a piecewise linear saturation model for the differential output current as a function of the differential input voltage, with a small-signal transconductance of g_m and a saturation voltage of V_{th} (the input voltage value at which all the current swings to one side, i.e., $g_m V_{th} = \frac{I_{bias}}{2}$). Let V_i be the output voltage of each node. Further, let us assume that in steady state, the oscillator is at a frequency of ω , and that $V_i = A\cos(\omega t + \phi_i)$, where A and ϕ_i are constants with respect to time. Note that from symmetry, the amplitudes of all nodes must be the same. If the quality factor (Q) of the resonant load is high, then the load filters out all harmonics except the fundamental. The node output voltage then equals the fundamental component of the nonlinear current times the load impedance at the oscillation frequency. This yields

$$\phi_i - \phi_{i-1} = \Delta\phi = \tan^{-1}\left(\frac{R}{\omega L}\left(1 - \frac{\omega^2}{\omega_0^2}\right)\right), \quad (1)$$

$$\frac{g_m R \cos\Delta\phi}{\pi}(\alpha + \sin(\alpha)) = 1, \quad (2)$$

where $\alpha = 2\sin^{-1}\left(\frac{V_{th}}{A}\right)$ and $\omega_0 = \frac{1}{\sqrt{LC}}$. (2) allows for the computation of the oscillation amplitude, while (1), in conjunction with the phase boundary condition, allows one to determine the oscillation frequency. Specifically, the phase shift around the ring must be an integral multiple of 2π , and therefore, $N\Delta\phi + \Delta\phi_{boundary} = 2i\pi$, $i \in I$, where $\Delta\phi_{boundary}$ is 0° or 180° , depending on the manner in which the ring is closed.

Intuitively, for $i = 0$, the boundary phase shift gets distributed among the elements of the ring. For example, an 8-element ring with boundary phase inversion produces an oscillation where the element phase shift $\Delta\phi$

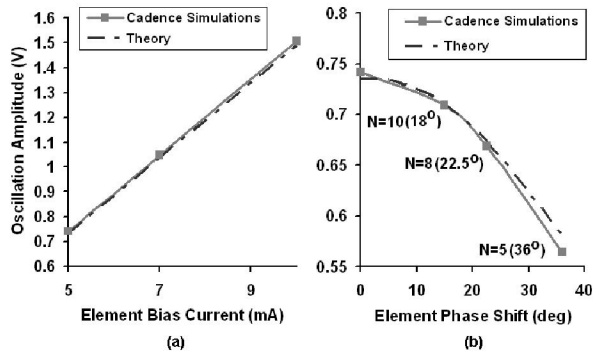


Fig. 2. (a) Oscillation amplitude for an 8-element ring versus element bias current. All elements are in phase since there is no phase inversion at the boundary. (b) Oscillation amplitude versus phase-shift per element for $I_{bias}=5$ mA.

is $-180^\circ/8 = -22.5^\circ$. Nonzero values of i produce other modes of oscillation; the orbital stability of those modes and their regions of attraction¹ are beyond the scope of this paper and will be dealt with in a future publication.

The oscillation amplitude, from (2), reduces to $A = \frac{2}{\pi} I_{bias} R \cos \Delta \phi$ for $A \gg V_{th}$. It does not depend on the number of stages, and linearly increases with bias current as expected. The amplitude decreases as $\Delta \phi$ increases, as the tuned loads function farther off their center frequency and present lower impedance.

To verify these results, simulations are carried out in Cadence using IBM's 8RF 0.13 μm CMOS process. The differential pair of each element consists of nMOS transistors with 100 fingers of width 0.48 μm , and an ideal tail current source is used. The tuned load's component values are $L = 4$ nH, $R = 240 \Omega$ and $C = 6.33$ pF, resulting in a center frequency of approximately 1 GHz and $Q=10$. Fig. 2(a) depicts the oscillation amplitude of an 8-element ring (with 0° element phase shift) for different element bias currents, while Fig. 2(b) depicts the amplitude for $I_{bias}=5$ mA for different element phase shifts, accomplished by providing a 180° phase inversion in the ring for different ring sizes. A good correlation is observed between the theoretical formulation² and Cadence simulations.

III. PHASE NOISE ANALYSIS

Two of the most widely accepted phase noise theories are the Linear Time-Variant (LTV) theory developed by Hajimiri and Lee [5], and the mathematically-rigorous theory developed by Demir and Roychowdhury [6]. In [7], the authors demonstrate the strong similarities between the two theories and the equivalence of the Perturbation Projection Vector (PPV), which is central to the latter theory, and the Impulse Sensitivity Function (ISF), which

¹The region of attraction of a stable point of a nonlinear system is defined as the set of initial conditions that cause the system to converge to the stable point at steady state.

²The piecewise linear model parameters g_m and V_{th} are computed for the different bias currents using standard short-channel MOSFET device equations.

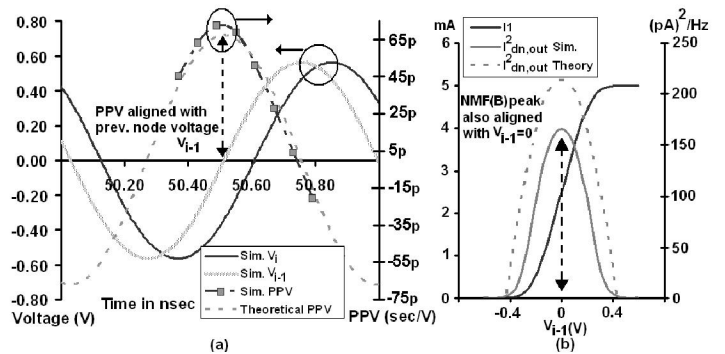


Fig. 3. (a) Comparison of theoretical PPV with Cadence simulations for a 5-element ring with 180° phase inversion (b) Differential pair output noise versus differential input voltage - theory versus simulations.

is employed in LTV theory. Both represent the time-dependent sensitivity of the oscillator's phase response to perturbations. In this paper, in favor of mathematical rigor, we will employ the latter theory. A detailed review of this theory is beyond the scope of this paper, and the reader is directed to [6] if the ensuing analysis seems unclear.

The *perturbed* first order differential equations for the i^{th} element of the tuned ring oscillator are given by

$$C \frac{dx_{2i}}{dt} + \frac{x_{2i-1}}{\omega L} + \frac{x_{2i}}{R} = f(x_{2i-2}) + n_i, \quad (3)$$

$$\frac{1}{\omega} \frac{dx_{2i-1}}{dt} = x_{2i}. \quad (4)$$

where f represents the piecewise linear saturation model, $x_{2i}(t)$ is the node output voltage ($V_i(t)$) and $x_{2i-1}(t)$ is its integral with respect to time normalized with respect to the oscillation frequency ($\omega \int V_i dt$). $n_i(t)$ is the noise current injecting into the i^{th} load; assuming that this noise arises from the devices of the transconductance cell of the i^{th} node alone³, $n_i(t)$ can be written as $B(x_{2i-2}(t), x_{2i-1}(t), x_{2i}(t))b_i(t)$, with $(b_i(t))_{i=1..N}$ being a vector of uncorrelated Gaussian white noise sources of unit variance and $B(x_{2i-2}(t), x_{2i-1}(t), x_{2i}(t))$ capturing the instantaneous current-and-voltage-dependent modulation (i.e. the cyclostationary effect) thus serving the purpose of the Noise Modulating Function (NMF) in [5].

The *unperturbed* steady state solution can be written as $x_{2i-1_s} = A \sin(\omega t + (i-1)\Delta\phi)$, $x_{2i_s} = A \cos(\omega t + (i-1)\Delta\phi)$, with A , ω and $\Delta\phi$ taking the values described in Section I. The PPV is determined by

1. forming the differential equations describing the *deviation* from the unperturbed steady state due to the noise perturbations,

2. forming the adjoint system to those equations and

3. determining the periodic solution to the adjoint system, normalized to $\dot{x}_s(0)$ (the derivative of the steady state solution vector at $t = 0$). This periodic solution is the PPV.

³This is reasonable as other sources of noise such as power supply noise, tail current noise and resonator noise can be minimized through proper design. Noise leakage from the transconductance cells of other nodes will be negligible if device parasitics are small.

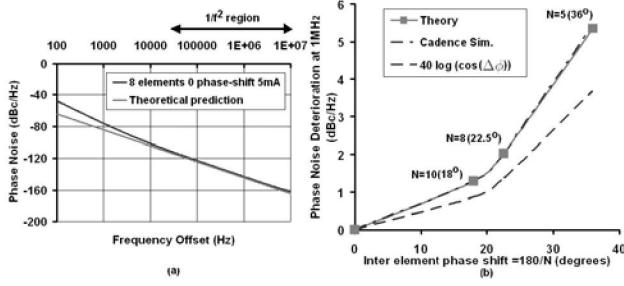


Fig. 4. (a) Theoretical and simulated phase noise for an 8-element ring with no phase shift (b) Phase noise difference at 1 MHz offset for rings with and without 180° phase-inversion.

Following these steps, the PPV, denoted by the vector $v(t)^4$, is determined to be

$$v_{2i-1} = \frac{1}{NA\omega\cos\Delta\phi} \cos(\omega t + (i-2)\Delta\phi), \quad (5)$$

$$v_{2i} = -\frac{1}{NA\omega\cos\Delta\phi} \sin(\omega t + (i-2)\Delta\phi). \quad (6)$$

To verify these results, a 5-element ring with 180° phase inversion (element phase shift = 36°) and elements identical to those described in Section II ($I_{bias}=5$ mA) is constructed in Cadence. The PPV component for the voltage of one of the elements is determined using the "Direct Measurement of Impulse Response" technique [5]⁵ and is compared to the theory in Fig. 3(a). An excellent agreement is seen. It is interesting to note that the PPV's peak is aligned with the zero crossings of the *voltage of the previous node*, rather than the node's own voltage, unlike traditional LC oscillators that function at the center frequency of the load.

To determine the NMF, B , we must find the differential output noise current of the differential pair of Fig. 1(a) as function of the instantaneous currents and voltages. Note that only the drain current thermal noise is considered in this treatment. Other noise sources, such as gate resistance noise, can be treated in a similar fashion. Performing small signal analysis at a general time instant, we have,

$$I_{dn,out} = \frac{g_{m1}(t)I_{dn2}}{g_{m1}(t) + g_{m2}(t)} + \frac{g_{m2}(t)I_{dn1}}{g_{m1}(t) + g_{m2}(t)} \quad (7)$$

where I_{dn1} and I_{dn2} are the time-varying drain thermal noise currents of the devices in the rms sense. The time-dependent device transconductances ($g_{m1}(t), g_{m2}(t)$) can be determined using standard short-channel device models. The bias dependent drain current thermal noise power of the FETs of the 0.13 μm process is characterized. There is a strong dependence on V_{gs} , while the variation with V_{ds}

⁴Note that odd-indexed elements of the PPV ($v_1(t), v_3(t), \dots$) are inconsequential since there is no noise associated with (4).

⁵Due to the equivalence of the ISF and the PPV, the PPV may also be measured in this way.

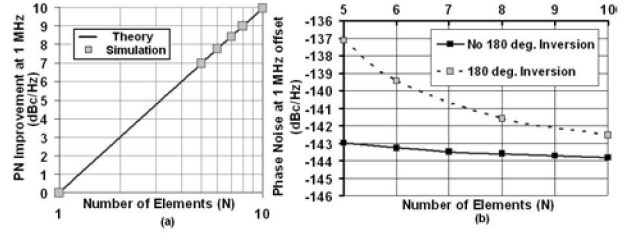


Fig. 5. (a) Simulated phase noise at 1 MHz offset for rings of different sizes with no phase shift ($I_{bias} = 5$ mA per element) (b) Simulated phase noise at 1 MHz offset with a fixed current budget ($I_{bias} = \frac{50}{N}$ mA per element).

is weak, as expected. Hence, for analysis purposes, the noise power is approximated with a piecewise linear fit with respect to V_{gs} ; Since device transconductance also primarily depends on V_{gs} , the differential output noise current $I_{dn,out}$ of stage i is primarily a function of the input voltage $x_{2i-2} = V_{i-1}$. Fig. 3(b) shows the theoretical $I_{dn,out}$ as a function of V_{i-1} to Cadence simulations for $I_{bias}=5$ mA. A reasonable match is observed and this curve is the NMF $B(x_{2i-2}(t))$ for the i^{th} element.

The output noise is maximum when the differential input is 0, and decreases as the input swings. When all the current has swung to one side, say FET 2, the output noise current drops to 0, since $g_{m1} = 0$ and $I_{dn1} = 0$. The PPV/ISF is also maximum when the differential input is 0 - hence, due the alignment of the peaks of the PPV and the NMF, the differential pair based ring oscillator *does not* possess good cyclo-stationary noise properties.

Using these formulations for the PPV and the NMF, the single-sideband phase noise spectrum of the tuned ring oscillator in the $\frac{1}{f^2}$ -region in dBc/Hz is given by [6]

$$\mathcal{L}(\Delta f) \approx 10\log_{10}\left(\frac{f^2 c}{\Delta f^2}\right), \quad (8)$$

$$c = \frac{1}{2\pi NC^2 A^2 \omega^2 \cos^2 \Delta\phi} \int_0^{2\pi} \sin^2 \theta B(A \cos \theta) d\theta, \quad (9)$$

where $f = \frac{\omega}{2\pi}$. As expected, phase noise improves with an increase in amplitude A . Further, as N is increased, the phase noise improves by a factor of $10\log_{10}N$. This is because the PPV's inverse- N dependence causes a $10\log_{10}N^2$ phase noise drop, but the number of noise sources in the circuit has increased by a factor of N , causing an overall improvement of $10\log_{10}N$. Finally, as the inter element phase shift is increased, the phase noise deteriorates due to the $\cos^2 \Delta\phi$ term in the denominator, the reduction of oscillation amplitude (which contributes another $\cos^2 \Delta\phi$ as seen in section I) and the integral term.

IV. EXPERIMENTAL VERIFICATION

Fig. 4(a) depicts the theoretical and simulated phase noise of a ring with 8 elements, no inter element phase shift and $I_{bias}=5$ mA. An close match is seen in the $\frac{1}{f^2}$ -region, revealing that the theory is able to predict the phase noise to an accuracy of 1.5 dB.

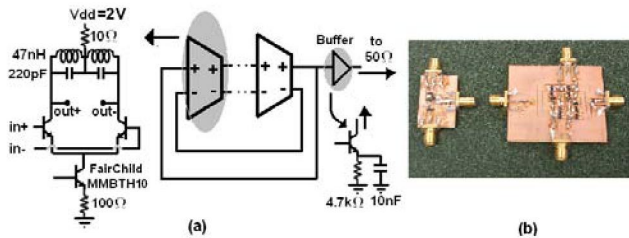


Fig. 6. (a) Circuit diagram for 50 MHz prototype oscillators (b) Photograph of prototype oscillators.

Fig. 4(b) depicts the phase noise difference for rings of different sizes with and without boundary phase inversion ($I_{bias}=5$ mA) at 1 MHz offset (which lies in the $\frac{1}{f^2}$ -region) to determine the effect of inter element phase shift. Fig. 5(a) depicts the phase noise improvement of rings of different sizes with $I_{bias}=5$ mA and no boundary phase inversion over a single element ring⁶. Once again, there is an extremely good match to the theoretical prediction. Note that Fig. 4(b) also depicts the contribution of $A^2 \cos^2 \Delta \phi$ in the denominator of (9) to the phase noise degradation due to inter element phase shift; the remaining degradation is due to the integral term.

Fig. 5(b) shows the simulated phase noise at 1 MHz offset for rings of different sizes without boundary phase inversion for a fixed current budget of 50 mA ($I_{bias} = \frac{50}{N}$ mA per element). The resonant load parameters are scaled as $L = N \times 0.4$ nH and $C = \frac{63.3}{N}$ pF to maintain a constant oscillation frequency. Assuming a constant quality factor of 10, the parallel resistance would scale as $R = N \times 24 \Omega$ and the oscillation amplitude would remain the same. (9) then dictates that the phase noise would remain roughly constant as the NMF, B , would scale down by a factor of N due to the decreasing current in each stage, thus cancelling the effect of NC^2 in the denominator. If boundary phase inversion is present, rings of lower sizes would experience phase noise deterioration due to the larger inter element phase shift. This deterioration would be identical to that described in the previous section and depicted in Fig. 4(b). The simulation results confirm these conclusions. Hence, if a phase resolution of 36° is desired for an application with a fixed current budget, the phase noise is better (by 5.5 dB in this case) if one uses alternate node voltages of a 10-element ring with boundary phase inversion as opposed to a 5-element ring.

To further validate the theoretical and simulated results, prototype 50 MHz oscillators are built on printed circuit boards (PCBs) using Fairchild's MMBTH10 BJTs ($f_T=650$ MHz). The first is a single element ring (i.e. cross-coupled oscillator) while the second is a 4-element ring with no boundary phase inversion. Fig. 6(a) depicts the circuit diagrams, while 6(b) is a photograph of the prototypes. Fig. 7 shows the measured phase noise of both oscillators for a bias-current of 1.25 mA per element. In

⁶A 1-element ring with no boundary phase inversion is nothing but a cross-coupled LC oscillator

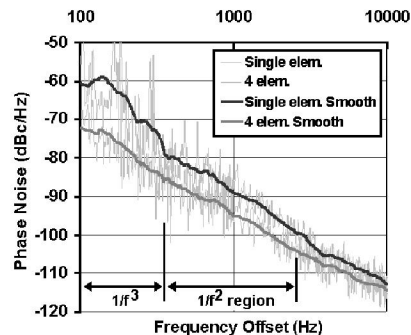


Fig. 7. Measured phase noise for both oscillators for a bias current of 1.25 mA per differential pair.

the $\frac{1}{f^2}$ region, the average phase noise difference is 6 dB, which matches the expected difference ($10 \log(4) = 6$ dB). The maximum and minimum phase noise differences in that region are 7.82 dB and 4.3dB respectively. The phase noise performance of the oscillators in the $\frac{1}{f^3}$ region is beyond the scope of this paper. The limited range of frequency offsets before the phase noise curves approach the thermal noise floor is a function of the low frequency of oscillation.

V. CONCLUSION

A rigorous phase noise theory for tuned ring oscillators is developed with a focus on the dependence of phase noise on the number of ring elements and inter element phase shift. It is seen that an increase in the number of elements N leads to a $10 \log_{10} N$ phase noise improvement, while an increase in inter element phase shift leads to phase noise deterioration. For multiple phase generation, under a fixed current budget, it is beneficial to use a larger ring sizes. Extensive simulations and experiments using prototype oscillators validate these claims.

REFERENCES

- [1] H. Hashemi, X. Guan and A. Hajimiri, "A Fully Integrated 24GHz 8-Path Phased-Array Receiver in Silicon," *ISSCC Dig. Tech. Papers*, pp. 390-391, Feb 2004.
- [2] J. Savoj and B. Razavi, "A 10-Gb/s CMOS clock and data recovery circuit with a half-rate binary phase/frequency detector," *IEEE JSSC*, vol. 38, no. 1, pp. 1321, Jan. 2003.
- [3] D. K. Ma and J. R. Long, "A subharmonically injected LC delay line oscillator for 17-GHz quadrature LO generation," *IEEE JSSC*, vol. 39, no. 9, pp. 1434-1445, Sep. 2004.
- [4] A. Hajimiri, S. Limotyrakis and T. H. Lee, "Jitter and phase noise in ring oscillators," *IEEE JSSC*, vol. 34, no. 6, pp. 790-804, June. 1999.
- [5] A. Hajimiri and T. H. Lee, "A General Theory of Phase Noise in Electrical Oscillators," *IEEE JSSC*, vol. 33, pp. 1791-194, Feb. 1998.
- [6] A. Demir, A. Mehrotra and J. Roychowdhury, "Phase noise in Oscillators: A Unifying Theory and Numerical Methods for Characterization," *IEEE Trans. on Circuits and Systems I*, vol. 48, no. 5, pp. 578-594, May 2001.
- [7] P. Vanassche, G. Gielen and W. Sansen, "On the Difference between Two Widely Publicized Methods for Analyzing Oscillator Phase Behavior," *IEEE/ACM International Conference on Computer Aided Design*, pp. 229-233, Nov. 2002.